Flexible Power Fabrics Made of Carbon Nanotubes for Harvesting Thermoelectricity

Suk Lae Kim, Kyungwho Choi, Abdullah Tazebay, and Choongho Yu*

Department of Mechanical Engineering Texas A&M University College Station, Texas 77843, United States

ABSTRACT

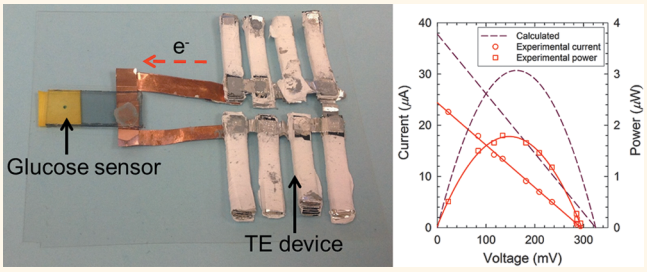

Thermoelectric energy conversion is very effective in capturing low-grade waste heat to supply electricity particularly to small devices such as sensors, wireless communication units, and wearable electronics. Conventional thermoelectric materials, however, are often inadequately brittle, expensive, toxic, and heavy. We developed both p- and n-type fabric-like flexible lightweight materials by functionalizing the large surfaces and junctions in carbon nanotube (CNT) mats. The poor thermopower and only p-type characteristics of typical CNTs have been converted into both p- and n-type with high thermopower. The changes in the electronic band diagrams of the CNTs were experimentally investigated, elucidating the carrier type and relatively large thermopower values. With our optimized device design to maximally utilize temperature gradients, an electrochromic glucose sensor was successfully operated without batteries or external power supplies, demonstrating self-powering capability. While our fundamental study provides a method of tailoring electronic transport properties, our device-level integration shows the feasibility of harvesting electrical energy by attaching the device to even curved surfaces like human bodies.

KEYWORDS: thermoelectric · carbon nanotube · flexible · sensor · n-type

Thermoelectric (TE) devices directly convert heat energy into electrical energy and *vice versa* without moving parts and complicated components/structures. They are simply made by alternatively connecting solid-state p-type and n-type semiconductors in series. These unique characteristics make TE devices very attractive for compact power generation and cooling. It is also feasible to harvest low-grade heat (low exergy) to generate electricity. For instance, a TE device may provide enough power to a sensor for sensing and wireless communication without external power supplies. Exemplary applications include self-powered health monitoring for humans and buildings as well as gas/chemical detection without wiring. Current commercial TE devices typically consist of expensive, toxic, and heavy inorganic materials, hindering a full utilization of their unique benefits. Recently, there have been efforts to alleviate the problems by adopting p-type polymeric materials such as poly(3,4-ethylenedioxythiophene) and polyaniline due to their intrinsically low thermal conductivity.[1−8] N-type organic materials with decent thermopower values have rarely been reported.[7,9,10] Therefore, there has been no flexible and lightweight organic thermoelectric devices generating enough power to operate an actual working device.

Here we successfully demonstrated that carbon nanotubes (CNTs) can be made into both p- and n-type materials with relatively high thermopower and thereby a CNT-based thermoelectric device can generate enough power to operate an electrochromic glucose

* Address correspondence to chyu@tamu.edu.

Received for review November 13, 2013 and accepted February 11, 2014.

Published online February 11, 2014
10.1021/nn405893t

sensor. In fact, CNTs have been excluded from thermoelectric materials due to the high thermal conductivity ($\sim 10^3$ W/(m K) at room temperature[11]) of individual CNTs, which is disadvantageous for creating a large temperature gradients necessary to obtain a large thermoelectric voltage. Moreover, individual CNTs exposed to air show only p-type behaviors with small thermopower values.[11] This work presents that these drawbacks of CNTs for thermoelectrics have been overcome by properly designing the junctions between CNTs and the surface of CNTs as well as making many junctions in their films (or mats) through rigorous debundling processes. When CNT surfaces are functionalized by molecules or chemical agents, electronic transport across CNT−molecule−CNT junctions can be optimized to increase thermopower by creating a small energy barrier. The presence of the junctions can also play a significant role in deterring phonon transport due to dissimilar vibrational characteristics between CNTs and molecules.

We present not only synthesis and characterization of both p- and n-type, flexible, and CNT-based thermoelectric materials, but also design and fabrication of TE modules to maximize electricity generation. More importantly, the TE device has been tested for operating a glucose sensor, demonstrating the feasibility of using the device for practical applications. For p-type materials, oxygen-doped CNTs were functionalized with sodium dodecylbenzenesulfonate (SDBS) to control thermopower as well as separate CNT bundles. Multiple dopants, polyethylenimine (PEI), diethylenetriamine (DETA), and $NaBH_4$ were utilized for maximizing n-type characteristics. It has been shown that PEI is effective to make n-type CNTs,[7,9,10] but the large molecules are electrically insulating, resulting in a reduction of electrical conductivity. Here, we used shorter DETA molecules composed of amine groups containing lone pairs of electrons so as not to considerably sacrifice electrical conductivity.

The n-type conversion mechanism and the role of the molecules coated on CNTs by the functionalization were thoroughly explained with a complete picture of electronic band diagrams in conjunction with electronic transport properties, which are of great importance in understanding the behaviors but have been barely studied in the past. The highest occupied molecular orbital (HOMO) and lowest unoccupied molecular orbital (LUMO) energy levels were found by performing cyclic voltammetry (CV) and ultraviolet−visible-infrared (UV−vis-IR) spectroscopy. The Fermi level was determined by using a Kelvin probe method, and the Hall measurement was carried out to obtain the type of carrier (electron or hole) as well as free carrier mobility. The following describe material synthesis, characterization, device design, and sensor operation.

RESULTS AND DISCUSSION

The p-type modules were made of as-purchased CNTs by filtering aqueous solutions containing CNTs dispersed by SDBS. When CNTs are exposed to air, they become p-type due to oxygen doping without any additional chemical treatments.[1−3,9,10,12−14] In this study, we used CNTs synthesized by a chemical vapor deposition (CVD) method in order to obtain a relatively high thermopower. According to our previous study,[14] it was found that single-wall CNTs grown by a CVD method exhibit relatively high thermopower than those grown by an arc discharge method and a high pressure carbon monoxide method.

While thermoelectric properties of individual CNTs are strongly affected by chirality and the number of walls, a bulk form of CNTs, typically called a CNT mat (or film) has electrical properties dissimilar to those of individual CNTs. Thermoelectric properties of a CNT mat are strongly affected by the degree of dispersion and the type of dispersants as well as junctions between CNTs. While it is feasible to increase the electrical conductivity of CNT mats up to $\sim 7 \times 10^4$ S/m with SDBS,[14] the focus of this study is to increase thermopower for high output voltage. We thickened the SDBS junction between CNTs using a 3:1 weight ratio of SDBS to CNT, so as to raise thermopower up to 97 μV/K (with 1.1×10^4 S/m), which is higher than our previous experimental result, 44 μV/K with a 2:1 weight ratio of SDBS to CNT.

Air-exposed CNTs were reduced by using PEI and DETA with subsequent $NaBH_4$ treatment in order to make n-type modules. When PEI coats CNTs, p-type CNTs were effectively converted to n-type.[7,9,10] However, PEI is electrically insulating and thereby deters electronic transport at the junction between CNTs. This is related to a large molecular weight (*i.e.*, long chain) of PEI, increasing the thickness of electrically insulating coating layers. To alleviate this problem, DETA, a short molecule with similar to the structure of PEI, was introduced. The nitrogen in DETA can play a role in n-type doping like PEI.[15]

The weight ratio of PEI to DETA was varied in order to find a ratio maximizing the power factor ($S^2\sigma$, where S and σ stand for thermopower and electrical conductivity, respectively). When 33 wt % PEI was replaced by DETA, the electrical conductivity was improved to 3900 from 3100 S/m of a 100 wt % PEI sample, as depicted in Figure 1. At the same time, thermopower was also improved to -63 μV/K, presumably due to small molecules additionally attached to CNT surfaces that are inaccessible by large PEI molecules. Nevertheless, with larger amounts (50 and 67 wt %) of DETA, the absolute value of thermopower was decreased with electrical conductivity reductions. We believe this is caused by weak doping from DETA. With only DETA as a doping agent, the typical thermopower value of CNT

mats (~40 μV/K)[14] were diminished to 8.4 μV/K, but thermopower values were still positive, suggesting the presence of mixed free carriers (holes and electrons). We believe that the mixed carriers decreased the electrical conductivity with the DETA ratios higher than 33%. The sample doped by 67/33 wt % PEI/DETA was additionally reduced by $NaBH_4$, and the electrical conductivity and thermopower were further improved to 5200 S/m and −86 μV/K, respectively. This resulted in an increase of the power factor to 38 μW/(m K^2), compared to that of the sample doped by only PEI, as shown in the inset of Figure 1.

Thermopower contains two contributions from holes and electrons with opposite signs. When two different types of carriers are present, thermopower can be described as

$$S = (S_e\sigma_e + S_h\sigma_h)/\sigma \quad (1)$$

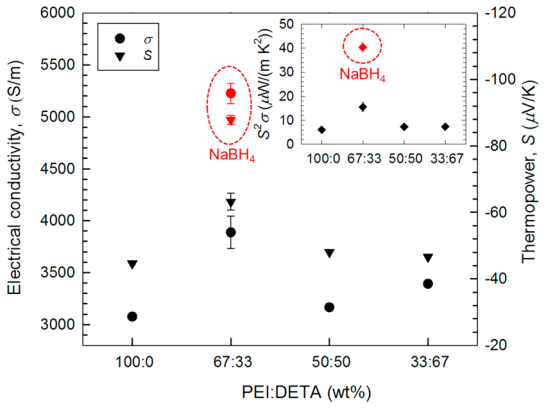

Figure 1. Electrical conductivity (circle) and thermopower (triangle) of the n-type CNT films with different PEI to DETA weight ratios. The inset shows the thermoelectric power factors ($S^2\sigma$). The samples with the PEI:DETA of 67:33 were further reduced by $NaBH_4$. The average measurement values and error bars for the samples with the PEI:DETA of 67:33 were obtained from three different samples.

where S_e and S_h stand for thermopower due to electrons and holes, respectively; σ_e and σ_h stand for electrical conductivity due to electrons and holes, respectively; and σ is the electrical conductivity due to both electron and hole carriers. When the contribution from electrons becomes dominant, the first term in eq 1 plays a major role, resulting in negative thermopower values. On the other hand, when the contributions from electrons and holes are comparable, thermopower becomes small due to the negative S_e and positive S_h. The increase of both electrical conductivity and thermopower is likely to be caused by the van Hove singularity in CNTs. When the Fermi level is raised toward the band edge, thermopower becomes larger due to the asymmetry in the differential electrical conductivity of CNTs.[12]

The presence of PEI in the samples was confirmed by scanning electron micrographs (SEMs) and Fourier transform infrared (FTIR) spectra. Panels a and b of Figure 2, respectively, show a cold-fractured cross section of p- and n-type CNT films. The tubular structures with relatively small diameters in the p-type CNT sample were clearly observed as opposed to the n-type CNTs whose diameters are relative large due to PEI and DETA coating layers. The n-type CNTs are well embedded in the film, which indicate PEI/DETA coated most of exposed CNT surfaces with relatively thick coating layers. If the coating is not uniform, some of CNTs would have been pulled out from the surface like Figure 2a. The insets also show the diameter change after the doping process. Similar features were also observed in the micrographs of the film surfaces, as shown in Figure 2c (p-type CNTs) and Figure 2d (n-type CNTs).

Figure 2e shows FTIR spectra of p-type CNT, PEI-doped CNT, and PEI/DETA-doped CNT films. When FTIR spectra from p-type CNTs are compared with those of PEI-doped and PEI/DETA-doped CNTs, distinct

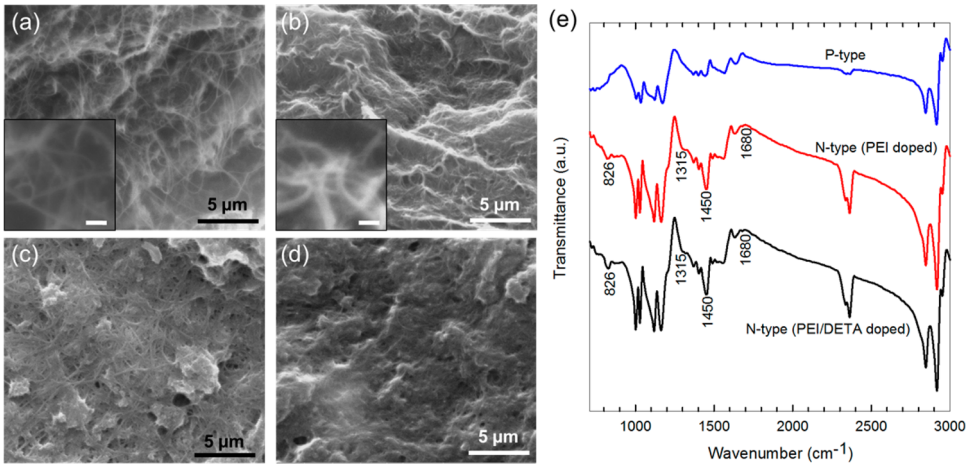

Figure 2. Cold-fractured cross sections of a p-type (a) and an n-type (b) CNT film. The scale bars in the insets indicate 100 nm. The film surface of a p-type film (c) and an n-type film (d). FTIR spectra of a p-type CNT, PEI-doped CNT, and PEI/DETA-doped CNT films (e).

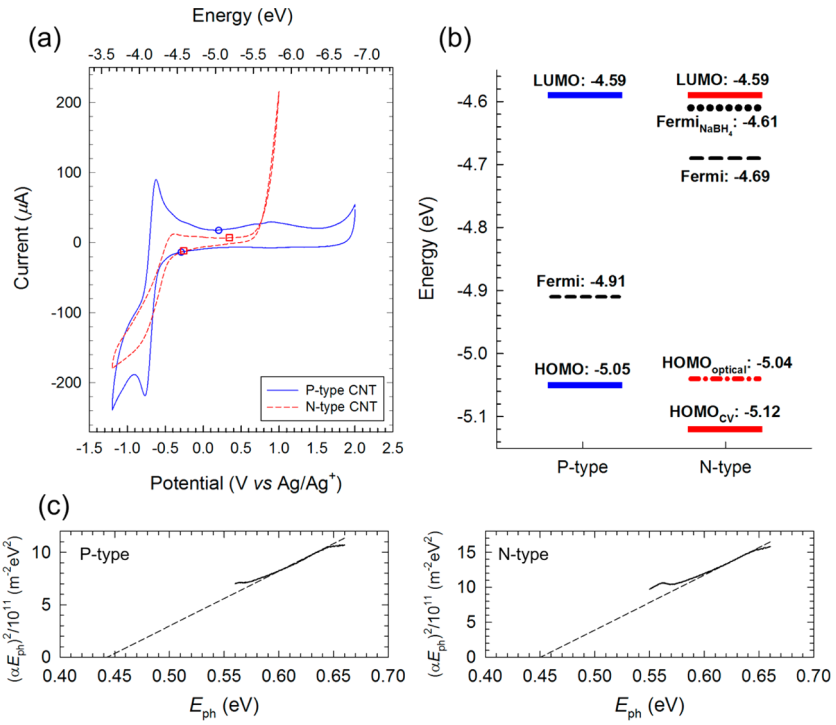

Figure 3. (a) Representative cyclic voltammograms of p- and n-type CNT films on a glassy carbon electrode (*vs* Ag/Ag^+ in acetonitrile solution with 0.1 M hexafluorophosphate (Bu_4NPF_6) as a supporting electrolyte, at a scan speed of 20 mV s^{-1}). The onset potentials of oxidation and reduction are indicated by circles (p-type) and squares (n-type). (b) HOMO, LUMO, and the Fermi level of p- and n-type CNT films. Two HOMO locations obtained by CV and UV−vis-IR results are indicated. The Fermi level from PEI/DETA doping (long dash) was moved up toward the vacuum level after additional $NaBH_4$ doping (dotted) was performed. (c) Tauc and Davis−Mott plots: $(\alpha E_{ph})^2$ as a function of E_{ph} calculated from UV−vis-IR transmission spectra (solid lines) of p- and n-type CNT films. The crossover points of extended slopes (broken lines) with E_{ph} indicate the band gap. The absorption coefficient, α, was set to 2.

absorption peaks coming from PEI and DETA (nitrogen-containing groups) were observed. The absorption peaks at 826 and 1680 cm^{-1}, respectively, suggest an out-of-plane bending (or NH_2 wag) and an in-plane NH_2 bending mode.[16−18] The absorption peak at 1315 cm^{-1} corresponds to secondary C−N stretch. An increase of the absorption peak at 1450 cm^{-1} with PEI and DETA compared to neighboring peaks may be due to primary C−N stretch.[18−20] Since PEI and DETA have similar chemical structures, their peaks are indistinguishable.

The electronic band diagrams of CNTs after doping with PEI/DETA or/and $NaBH_4$ were investigated by using CV, UV−vis-IR, and Kelvin probe measurement data so as to understand n-type conversion mechanism (see Figures S1−S3 in Supporting Information for details). The HOMO and LUMO energy levels were found from the onset potentials of oxidation and reduction in CV data, shown in Figure 3a, using ferrocene as an external standard[21,22] (see Supporting Information Figure S1). For p-type CNTs, HOMO and LUMO were estimated to be −5.05 and −4.59 eV from the vacuum level (0 eV), as shown in Figure 3b. The HOMO and LUMO of n-type CNTs were almost constant with a small change in the HOMO level to −5.12 eV, resulting in a larger band gap (0.53 eV) compared to 0.46 eV from the p-type CNTs.

Optical band gaps were found using UV−vis-IR spectra from the crossover points of the slopes with the *x*-axis,[23] as shown in Figure 3c (see Supporting Information Figure S2 for transmittance data). The p-type CNTs show 0.44 eV, which is very similar to the band gap measured by CV. On the other hand, the n-type optical band gap (0.45 eV) was found to be smaller by 0.08 eV, compared to that from the CV results. In the optical method, visible and infrared light energy is absorbed by both CNTs and PEI/DETA as the light passes through the samples. On the other hand, the electrochemical method relies on the charge interaction between an electrolyte and sample surfaces, and the presence of electrically insulating PEI/DETA coating layers on CNTs may have affected the measurement results. This difference in the two techniques could be the reason for the small discrepancy of the band gap measurement results. Considering the optical band gap, the HOMO of n-type CNTs could be located at −5.04 eV since LUMO is not likely to be raised toward the vacuum level by the donation of electrons from PEI/DETA.

On the basis of the band gap information, the location of the Fermi energy determines the type (p or n) of CNTs. In our study, a contact potential difference (CPD), which is the work function (WF) difference between a probe and a sample, was measured

TABLE 1. Physical Properties of p- and n-Type CNT Films

sample	oxidation onset/V	reduction onset/V	HOMO/eV	LUMO/eV	band gap (CV)/eV	band gap (optical)/eV	CPD/V	Fermi level/V
p-type	0.21	−0.25	−5.05	−4.59	0.46	0.44	0.04	−4.91
n-type	0.28	−0.25	−5.12	−4.59	0.53	0.45	0.26 (0.34)[a]	−4.69 (−4.61)[a]

[a] PEI/DETA-doped CNT samples were further reduced by $NaBH_4$.

TABLE 2. Hall Measurement Results of p- and n-Type CNT Films

sample	sheet resistance/Ω	hall voltage[a]/μV	carrier concentration/cm^{-3}	mobility/$cm^2\ V^{-1}\ s^{-1}$	majority carrier
p-type	11.5	+8.5	1.86×10^{21}	0.365	hole
n-type	30.3	−12.6	1.25×10^{21}	0.206	electron

[a] Hall voltage was measured with 20 mA under 10120 G.

by using the Kelvin probe method in air environment (see Supporting Information Figure S3 for CPD data). Since the WF of a probe tip may be affected by moisture and other contaminants in air, the CPD of a gold foil was measured for calibration, which was found to be −150 mV. If we assume that the Fermi level of the gold foil is located at −5.10 eV,[24−26] the Fermi levels of p- and n-type CNTs are estimated to be −4.91 and −4.69 eV, respectively, as shown in Figure 3b. The Fermi levels of p- and n-type CNTs are, respectively, close to the HOMO and LUMO, which explains the n-type conversion (negative thermopower values) of air exposed p-type CNTs. It was also found that the $NaBH_4$ treatments further shifted the Fermi level (−4.61 eV) toward LUMO, indicating stronger n-type conversion upon reduction by $NaBH_4$. The physical properties of the p- and n-type CNTs are summarized in Table 1.

To have a complete picture of electronic behaviors upon doping, it is necessary to obtain free carrier mobility and concentrations. Therefore, we have performed both sheet resistance and hall measurements with the van der Pauw technique.[27,28] As summarized in Table 2, the hall voltages of p- and n-type CNTs were measured to be +8.50 and −12.6 μV with 20 mA, indicating that the majority carriers for p- and n-type are, respectively, holes and electrons. The carrier concentrations of p- and n-type CNTs were determined to be 1.86×10^{21} and 1.25×10^{21} cm^{-3}, respectively. The relatively high carrier concentration suggests that electron donations to CNTs due to the lone-pair of electrons from the repeating nitrogen in PEI and DETA are very effective. The n-type (0.206 $cm^2/(V\ s)$) mobility is smaller than that of p-type (0.365 $cm^2/(V\ s)$), presumably due to the PEI/DETA coating layers that impede carrier transport across the junctions between CNTs. This mobility is also much smaller than those of individual CNTs,[29] which is likely due to the junctions between tubes. This result implies it may be possible to further improve the electrical conductivity by using shorter (or smaller molecular weight) and/or electrically conducting molecules as dopants.

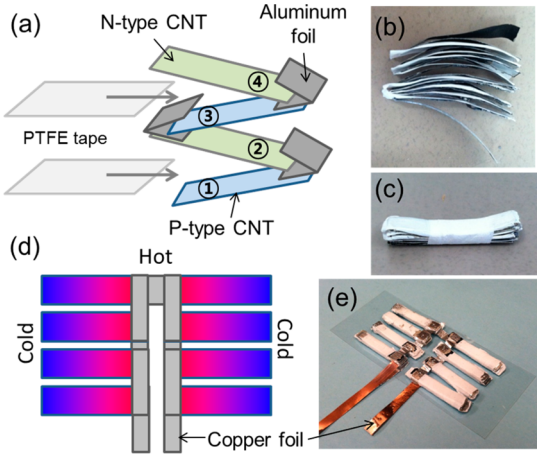

Figure 4. (a) Assembly process of p- and n-type carbon nanotube films. (b) One module (stack) consists of 9 p-type and 9 n-type films. (c) The module was bound by a PTFE tape. (d) A device design that maximizes thermoelectric voltage generation for a given temperature gradient, and (e) completed thermoelectric device consists of 144 films (72 p-type and 72 n-type).

The p- and n-type films were cut into 25 mm × 4.0 mm (called legs), and they were alternatively connected electrically in series and thermally in parallel with electrically insulating polytetrafluoroethylene (PTFE) films between the legs, as schematically depicted in Figure 4a. An as-assembled stack of legs (called a module) is shown in Figure 4b,c. Each module was connected in series by copper foils as schematically shown in Figure 4d. A picture of thermoelectric device is shown in Figure 4e. This device architecture is to maximize thermoelectric voltage determined by thermopower ($S_{p\ or\ n}$) and temperature gradient between hot and cold sides ($\Delta T_{i\ or\ j}$) as well as the number of legs. The total thermoelectric voltage (V_{TE}) generated from the device can be described as

$$|V_{TE}| = N_m[\sum_{i=1,3,5,\ldots}^{N_l-1} |S_p \Delta T_i| + \sum_{j=2,4,6,\ldots}^{N_l} |S_n \Delta T_j|] \quad (2)$$

where N_m and N_l, respectively, indicate the numbers of modules and legs in each module; the subscripts, p and

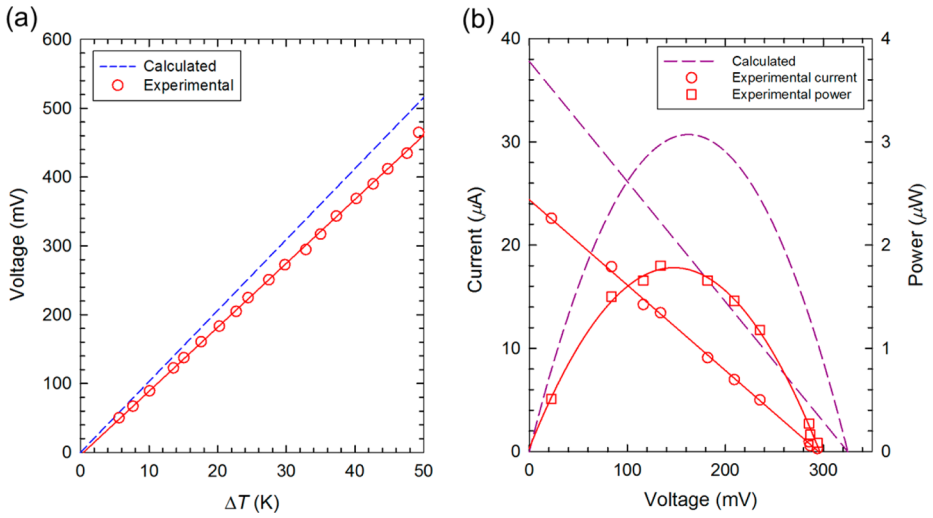

Figure 5. (a) Thermoelectric voltage generated by thermoelectric device as a function of temperature gradient. The discrepancy between the experimental values (circle) and the calculated voltage (short dash) would be due to misalignment during module assembly that created temperature drops in the hot side of the module. (b) Current−voltage and power output with varying load conditions at a ΔT= 32 K for operating an electrochromic glucose sensor. The calculated values (long dash) were obtained by assuming electrical contact resistance is negligible, suggesting further improvement in power output with an optimized assembly process.

n indicate p- and n-type; ΔT_i and ΔT_j stand for the temperature gradient along the long edge of a leg indexed from the bottom to the top as shown in Figure 4a.

The center part of the device was mounted on a heating block, where top and bottom aluminum blocks were heated to create temperature gradients (see the measurement setup in Supporting Information Figure S4). The output thermoelectric (open-circuit) voltage was measured to be ~9.3 mV/K, leading to 465 mV at ΔT = 49 K, as indicated by circles in Figure 5a. Load resistances were varied to record current as a function of the output voltage, and then the output power was plotted in Figure 5b. The advantage of the stacking method is to increase the voltage generated by each leg, but temperature drop (ΔT_{drop}) was created on the hot side due the thermal resistance. Note that the modules were clamped with a moderate pressure (approximately 700 N/m^2) in order to simulate normal operation in practice.

To estimate the temperature drop across each leg, the temperature of the top surface of a module was measured while the bottom part of the module was heated to 35, 45, and 55 °C. Assuming that there is a linear temperature drop along the thickness direction of the module at the heating side, the temperature at the middle of the stack in the heating side were estimated to be 31.6, 38.5, and 45.8 °C, respectively (see Supporting Information Figure S5 about temperature distributions along the thickness direction of the module). From the measurement data, ΔT_{drop} by each layer was estimated to be 4% of total temperature drop. The actual temperature ($T_{i,hot}$) on the hot side of ith leg from the bottom of each module can be calculated as $T_{1,hot} - 0.04 \times i \times \Delta T$. By considering the temperature drop in the modules, theoretical V_{TE} as a function of ΔT was obtained as shown in the blue short-dash line of Figure 5a. The small discrepancy may come from the misalignment of stacked legs in the modules during assembly.

The temperature drop comes from the thermal resistance ($R_{thermal}$) of the module along the thickness direction, which can be estimated by using a series resistor model.

$$R_{thermal} = \sum_{i=1}^{N_l} \frac{1}{A}\left(\frac{t_{PTFE}}{k_{PTFE}} + \frac{t_{Al}}{k_{Al}} + \frac{t_{CNT}}{k_{CNT}} + R_{contact}\right)_i \quad (3)$$

where A, t, and k indicate the thickness, thermal conductivity, area of the indexed materials, respectively; $R_{contact}$ is thermal contact resistance between the films. In the bracket of eq 3 is the thermal contact resistance mainly due to air trapped between the layers. Among the first three terms, thermal resistance from PTFE is dominant due to relatively thick layer (~220 μm), compared to Al (~20 μm) and CNT (8 μm). Assuming thermal conductivity of PTFE is ~0.25 W/(m K),[30] the first term in the bracket of eq 3 is estimated to be $\sim 9 \times 10^{-4}$ m^{2}K/W, which is comparable to typical thermal contact resistances between metallic interfaces under vacuum (*i.e.*, poor thermal contact).[31] This suggests that further optimized devices may yield a higher output voltage.

The output voltage of 150 mV from the thermoelectric device was selected for operating a glucose sensor based on the testing results of the sensor unit with a power supply. It was found that the electrochromic sensor worked properly with an input voltage of ~100 mV or higher. Therefore, we set our operation voltage slightly higher than 100 mV. To maximize

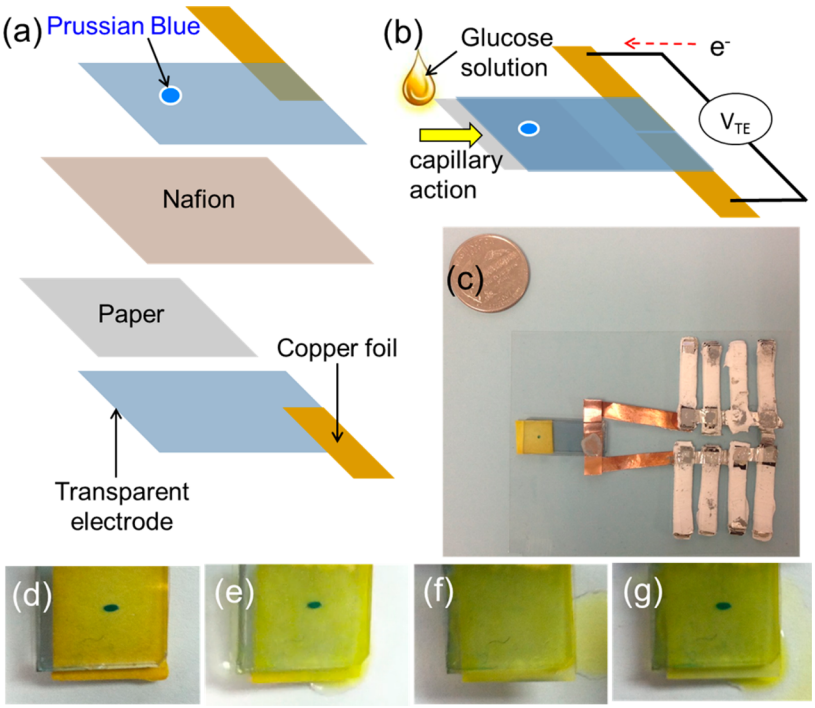

Figure 6. (a) Exploded view schematic of a glucose sensor with Prussian blue display. (b) Operation schematic of the glucose sensor with a thermoelectric device. (c) Prototype of glucose detection sensor integrated with a thermoelectric device. PB display of glucose sensor before (d) and after (e) injection of 50 μL of solution containing 0.2 mM glucose without supplying power. When power (150 mV) was supplied by the thermoelectric device, the PB disappeared after 180 s due to the change into PW (f). The PW changed back to blue after stop supplying power (g).

power output at an output voltage of 150 mV, an open circuit voltage (OCV) of 300 mV was chosen since the maximum power is obtained at a half of OCV. According to Figure 5a, it is necessary to have a temperature gradient of 32 K. The output current and power with a temperature gradient of 32 K were measured, showing 1.8 μW at the matching 150 mV in Figure 5b. This power output is orders of magnitude larger than those of other organic thermoelectrics,[4,32] which could be utilized for operating wireless communication devices. For instance, a TE powered sensor can send $\sim 10^3$ bits (125 bytes $\approx$ 125 text characters) of information per every 10 s wirelessly by accumulating 1 μW of energy to a capacitor.[33]

We also estimated the maximum power output can be 3.1 μW when the device is free of electrical contact resistance, misalignment, and defects with a temperature gradient of 32 K, as shown in the purple log-dash line of Figure 5b. The ideal device resistance from 72 p−n pairs was calculated to be 8.6 kΩ in comparison to 11.5 kΩ from our actual device for testing as the resistances of an individual p- and n-type leg were measured to be 38 and 81 Ω, respectively. If we assume the temperature gradient is higher (100 K) with the ideal device, the maximum output power could be as high as 31 μW (see Supporting Information Figure S6).

The thermoelectric device was tested for operating a glucose sensor so as to demonstrate that the power generation from our device is practically viable. The internal impedance of the sensor was designed to be close to the matching load resistance for an operation at the maximum power output. The glucose sensor consists of transparent electrodes, a Nafion membrane, and a paper, as shown in Figure 6a. The transparent electrodes were made of carbon nanotubes stabilized by poly(3,4-ethylenedioxythiophene):poly(styrenesulfonate) (PEDOT:PSS). On the electrode, we deposited electrochromic Prussian blue (PB), which reversibly changes color upon reaction only with a supply of current. Figure 6b illustrates the operation of the glucose sensor and Figure 6c shows a prototype by integrating the thermoelectric device. When a drop ($\sim$50 μL) of glucose solution containing 0.20 mM glucose is soaked by the paper, where $K_3Fe(CN)_6$ is loaded, due to a capillary action, $K_4Fe(CN)_6$ is produced without changing color before (Figure 6d) and after (Figure 6e) the glucose injection. Upon applying an electrical potential, potassium ions and electrons coming from oxidation of $K_4[Fe(CN)_6]_3$ turns $Fe(III)_4[Fe(II)(CN)_6]_3$(PB) into Prussian white (PW), $K_4Fe(II)_4[Fe(II)(CN)_6]_3$,[34] as shown in Figure 6f. After disconnecting the thermoelectric power source, PW returned to PB as shown in Figure 6g.

CONCLUSIONS

CNTs were functionalized to p- or n-type materials, and a TE device made of CNT films was designed and fabricated to operate a glucose sensor. The electronic

transport properties were controlled by adjusting the amount of coating on CNTs for p-type films as well as reducing CNTs with multiple agents, PEI, DETA, and $NaBH_4$ for n-type. When the mixing ratio of PEI to DETA (67:33 wt %) was optimized, n-type thermopower values as large as $-86\ \mu V/K$ at 5200 S/m were obtained due to synergistic effects from both large and small dopant molecules. According to Kelvin probe measurement results, the Fermi level of the p-type samples (-4.91 eV) were changed to -4.69 eV after PEI/DETA reduction and -4.61 eV after additional $NaBH_4$ reduction, clearly indicating n-type conversion after the doping processes. CV and UV−vis-IR measurement results suggest that the HOMO and LUMO energy levels are, respectively, located at -5.05 and -4.59 eV. Compared to free hole carrier mobility (0.365 $cm^2/(V\ s)$), the n-type CNT films showed a lower electron mobility (0.206 $cm^2/(V\ s)$) presumably due to the electrically insulating PEI/DETA that deter the carrier transport across the junctions between CNTs. The high free carrier concentrations ($1.86 \times 10^{21}\ cm^{-3}$ for p-type and $1.25 \times 10^{21}\ cm^{-3}$ for n-type) suggest that it is necessary to further increase the carrier mobility to obtain higher electrical conductivity.

The thermoelectric device was made of 72 p-type and 72 n-type CNT films electrically connected in series and thermally in parallel so as to maximally utilize temperature gradients. This device produced 465 mV at a temperature gradient of 49 K, which is much larger than those of other polymer based composites. The TE device was integrated with a glucose sensor and the self-powered sensor system was operated at a matching voltage of ~150 mV by a temperature gradient of 32 K. The power output was measured to be as high as 1.8 μW, which is practically viable for operating sensor units equipped with wireless communication and power management circuits. Further work may result in self-powered sensor systems for a wide range of applications including wearable electronics operated by body heat.

METHODS

Material Synthesis. CNTs purchased from CheapTubes, Inc. were used for all experimental work. According to manufacturer's specifications, CNTs were synthesized by a chemical vapor deposition method and contain approximately 50/50 wt % single/double-wall tubes with 99 wt % purity. The outer and inner diameters of the CNTs are 1−2 nm and 0.8−1.6 nm, respectively, and their lengths are 3−30 μm. Five milligrams of CNTs was dispersed in 20 mL of deionized (DI) water with 15 mg of SDBS (88%, Acros Organics) to prepare CNT solutions. Sonication was conducted in two modes, bath type sonicator (Branson 1510) for 6 h followed by a probe sonicator (Misonix Micron XL2000 Ultrasonic Homogenizer) for 2 h.

To synthesize p-type CNT films, the as-prepared CNT solution was vacuum-filtered onto a PTFE membrane (pore diameter, 0.45 μm; thickness, 45 μm, Tisch Scientific) with additional DI water, and subsequently the film was dried in air at 50 °C. For n-type CNT films, mixtures (1 g) of PEI (branched, molecular weight: 600, 99%, Alfar Aesar) and DETA (99%, Alfar Aesar) with PEI:DETA ratios of 100:0, 67:33, 50:50, and 33:67 were dissolved in 9 mL of DI water. This aqueous solution (10 g) was added to the CNT solutions (20.02 g). This mixture solution was stirred for 48 h at 50 °C, and then the solution was vacuum-filtered onto a PTFE membrane with additional DI water. Subsequently, the film was dried in air at 50 °C. For additional doping with sodium borohydride ($NaBH_4$, purity: 98%, Fisher Scientific), the dried film was immersed in an aqueous 1 M $NaBH_4$ solution for 24 h, and then dried in air at 50 °C. The thickness of the CNT layer in the film was measured to be 8 μm under a scanning electron microscope by inspecting cold-fractured cross sections of the CNT films.

Thermoelectric Device Fabrication. As-prepared CNT films on a PTFE membrane were cut into rectangular shapes 4 mm in width and 25 mm in length. Typical thickness of the CNT films was 8 μm. The thermoelectric modules were made by alternatively connecting p- and n-type CNT films electrically in series with aluminum foils using a silver adhesive (silver adhesive 503, electron microscopy sciences), and thermally in parallel by stacking 9 p-type and 9 n-type films. To avoid electrically connecting films in the stacking direction, PTFE tapes (75 μm thickness, McMaster Carr) were inserted between p- and n-type films. To maximize the voltage and power output, a total of eight modules (stacks) were connected electrically in series with an arrangement as shown in Figure 4d.

Glucose Sensor Fabrication. Transparent electrodes were prepared by spraying a mixture of 2 mg of CNTs and 10 g of PEDOT:PSS (Clevios PH1000, H.C. Starck) on glass slides (25 mm × 10 mm) at ~80 °C with a spray gun (0.2 mm nozzle diameter, GP-S1, Fuso Seiki Co.). The CNTs in the mixture were dispersed by the probe sonicator for 2 h prior to the spraying process. The sheet resistance of the transparent electrode was measured to be 1−1.5 kΩ/sq. For electro-depositing Prussian blue (PB) on the transparent electrode, a plating solution (100 mL) containing 2.6 mM HCl (36.5−38%, EMD Millipore), 10 mM $K_3Fe(CN)_6$ (98.5%, Acros Organics), and 10 mM $FeCl_3$ (98%, Alfar Asear) was freshly prepared. The electrode was covered by a PTFE tape with a 1 mm diameter hole, and subsequently immersed in the solution. PB was galvanostatically deposited by 0.4 $\mu A/mm^2$ for 30 s with Ag/AgCl as a reference electrode and Pt as a counter electrode. The glucose sensing paper was prepared by drop-casting 40 μL of a 0.01 M phosphate buffered saline (pH 7.4, ultra high purity grade, Amresco) containing 125 mM $K_3Fe(CN)_6$ and 500 unit (106 U/mg at 37 °C) of glucose oxidase (GOx, Amresco) onto a chromatographic paper (10 mm × 10 mm, Whatman). After it was dried at ambient air, the paper was sandwiched between the PB deposited electrode and a bare CNT electrode. A Nafion membrane (N-115, Dupont) was used for separating the sensing paper from the PB deposited electrode. The glucose solution contained 0.5 mM anhydrous D-(+)-glucose (99%, Alfa Aesar).

Electrical Property Measurements. Electrical properties of CNT films, including electrical conductivity and thermopower, were measured at room temperature along the in-plane direction. A four probe method was employed to obtain electrical conductivity from linear current−voltage relations by multiplying geometrical factors. For thermopower measurements, thermoelectric voltage across the sample was measured at 10 different temperature gradients between −10 and +10 K and then thermopower was obtained from the slope of temperature gradient-voltage data.

Sample Characterization. The surface and cross section of the carbon nanotube films were inspected by using a field-emission SEM (FEI Quanta 600). FTIR (Nicolet 380, Thermo Fisher Scientific) was performed in conjunction with attenuated total reflectance accessory (AVATAR OMNI Sampler, Germanium crystal) under an ambient condition. Electrochemical measurements were carried out with a CHI 600 electrochemical analyzer with a three-electrode system at a scanning rate of 20 mV/s in an

anhydrous acetonitrile solution (98%, Sigma-Aldrich) containing 0.1 M Bu_4NPF_6 (98%, Sigma-Aldrich) and 0.01 M $AgNO_3$ (99.9%, Alfa Aesar). A 70-sccm Ar was purged into the solution for 1 h to remove oxygen from the solution. A glassy carbon was used as a working electrode, a platinum-wire was used as the counter electrode, and an Ag/Ag^+ electrode was used as the reference electrode. When ferrocene was used as an external standard (−4.8 eV *vs* vacuum), the half wave potential $E_{1/2}(Fc/Fc^+)$ was measured to be −0.04 V *vs* Ag/Ag^+. For the electrochemical and UV−vis-IR measurements, samples were prepared by spraying the CNT-containing solutions on the glassy carbon or polished quartz substrates for 180 s (similar to the method for preparing the transparent electrodes). Transmittance was measured by using a UV−vis-NIR spectrophotometer (Hitachi U-4100). For Kelvin probe measurements, the local surface potential of the samples was measured with a Dimension Icon AFM (Bruker) using a Pt-coated cantilever with 30 nm lift height with a 75 kHz tapping mode. Sheet resistance and the Hall measurements with the Van der Pauw geometry (15 mm × 15 mm) were performed with a homemade setup following the ASTM F76-08 method.

Conflict of Interest: The authors declare no competing financial interest.

Acknowledgment. The authors gratefully acknowledge financial support from the U.S. Air Force Office of Scientific Research (Grant No. FA9550-13-1-0085) under the auspices of Dr. Charles Lee, the Pioneer Research Center Program through the National Research Foundation of Korea (Grant No. 2011-0001645) funded by the Ministry of Education, Science and Technology, and the US National Science Foundation (Grant No. CMMI 1030958).

Supporting Information Available: CV, UV−vis-IR, and Kelvin probe measurement data; the TE device setup; heat transfer experimental results of a thermoelectric module; current−voltage and power output at ΔT= 100 K. This material is available free of charge *via* the Internet at http://pubs.acs.org.

REFERENCES AND NOTES

1. Yu, C.; Kim, Y.; Kim, D.; Grunlan, J. C. Thermoelectric Behavior of Segregated-Network Polymer Nanocomposites. *Nano Lett.* **2008**, *8*, 4428–4432.
2. Yu, C.; Choi, K.; Yin, L.; Grunlan, J. C. Light-Weight Flexible Carbon Nanotube Based Organic Composites with Large Thermoelectric Power Factors. *ACS Nano* **2011**, *5*, 7885–7892.
3. Kim, D.; Kim, Y.; Choi, K.; Grunlan, J. C.; Yu, C. Improved Thermoelectric Behavior of Nanotube-Filled Polymer Composites with Poly(3,4-ethylenedioxythiophene) Poly(Styrenesulfonate). *ACS Nano* **2010**, *4*, 513–523.
4. Bubnova, O.; Khan, Z. U.; Malti, A.; Braun, S.; Fahlman, M.; Berggren, M.; Crispin, X. Optimization of the Thermoelectric Figure of Merit in the Conducting Polymer Poly(3,4-ethylenedioxythiophene). *Nat. Mater.* **2011**, *10*, 429–433.
5. Choi, K.; Yu, C. Highly Doped Carbon Nanotubes with Gold Nanoparticles and Their Influence on Electrical Conductivity and Thermopower of Nanocomposites. *PLoS One* **2012**, *7*, e44977.
6. Wang, H.; Yin, L.; Pu, X.; Yu, C. Facile Charge Carrier Adjustment for Improving Thermopower of Doped Polyaniline. *Polymer* **2013**, *54*, 1136–1140.
7. Freeman, D.; Choi, K.; Yu, C. N-Type Thermoelectric Performance of Functionalized Carbon Nanotube-Filled Polymer Composites. *PLoS One* **2012**, *7*, e47822.
8. Kim, Y. S.; Kim, D.; Martin, K. J.; Yu, C.; Grunlan, J. C. Influence of Stabilizer Concentration on Transport Behavior and Thermopower of Carbon Nanotube Filled Latex-Based Composites. *Macromol. Mater. Eng.* **2010**, *295*, 431–436.
9. Yu, C.; Murali, A.; Choi, K.; Ryu, Y. Air-Stable Fabric Thermoelectric Modules Made of N- and P-Type Carbon Nanotubes. *Energy Environ. Sci.* **2012**, *5*, 9481–9486.
10. Ryu, Y.; Freeman, D.; Yu, C. High Electrical Conductivity and N-Type Thermopower from Double-/Single-Wall Carbon Nanotubes by Manipulating Charge Interactions between Nanotubes and Organic/Inorganic Nanomaterials. *Carbon* **2011**, *49*, 4745–4751.
11. Yu, C.; Shi, L.; Yao, Z.; Li, D.; Majumdar, A. Thermal Conductance and Thermopower of an Individual Single-Wall Carbon Nanotube. *Nano Lett.* **2005**, *5*, 1842–1846.
12. Yu, C.; Ryu, Y.; Yin, L.; Yang, H. Modulating Electronic Transport Properties of Carbon Nanotubes and Improving the Thermoelectric Power Factor *via* Nanoparticle Decoration. *ACS Nano* **2011**, *5*, 1297–1303.
13. Collins, P. G.; Bradley, K.; Ishigami, M.; Zettl, A. Extreme Oxygen Sensitivity of Electronic Properties of Carbon Nanotubes. *Science* **2000**, *287*, 1801–1804.
14. Ryu, Y.; Yin, L.; Yu, C. Dramatic Electrical Conductivity Improvement of Carbon Nanotube Networks by Simultaneous De-Bundling and Hole-Doping with Chlorosulfonic Acid. *J. Mater. Chem.* **2012**, *22*, 6959–6964.
15. Valentini, L.; Armentano, I.; Puglia, D.; Kenny, J. M. Dynamics of Amine Functionalized Nanotubes/Epoxy Composites by Dielectric Relaxation Spectroscopy. *Carbon* **2004**, *42*, 323–329.
16. Vukovic, G. D.; Marinkovic, A. D.; Skapin, S. D.; Ristic, M. D.; Aleksic, R.; Peric-Grujic, A. A.; Uskokovic, P. S. Removal of Lead from Water by Amino Modified Multi-Walled Carbon Nanotubes. *Chem. Eng. J.* **2011**, *173*, 855–865.
17. Huang, Y. P.; Lin, I. J.; Chen, C. C.; Hsu, Y. C.; Chang, C. C.; Lee, M. J. Delivery of Small Interfering RNAs in Human Cervical Cancer Cells by Polyethylenimine-Functionalized Carbon Nanotubes. *Nanoscale Res. Lett.* **2013**, 8.
18. Smith, B. C. *Infrared Spectral Interpretation: A Systematic Approach*, 1st ed.; CRC Press: New York, 1998.
19. Basiuk, E. V.; Basiuk, V. A.; Banuelos, J. G.; Saniger-Blesa, J. M.; Pokrovskiy, V. A.; Gromovoy, T. Y.; Mischanchuk, A. V.; Mischanchuk, B. G. Interaction of Oxidized Single-Walled Carbon Nanotubes with Vaporous Aliphatic Amines. *J. Phys. Chem. B* **2002**, *106*, 1588–1597.
20. Misra, A.; Tyagi, P. K.; Singh, M. K.; Misra, D. S. Ftir Studies of Nitrogen Doped Carbon Nanotubes. *Diamond Relat. Mater.* **2006**, *15*, 385–388.
21. Gritzner, G.; Kuta, J. Recommendations on Reporting Electrode-Potentials in Nonaqueous Solvents (Recommendations 1983). *Pure Appl. Chem.* **1984**, *56*, 461–466.
22. Bredas, J. L.; Silbey, R.; Boudreaux, D. S.; Chance, R. R. Chain-Length Dependence of Electronic and Electrochemical Properties of Conjugated Systems—Polyacetylene, Polyphenylene, Polythiophene, and Polypyrrole. *J. Am. Chem. Soc.* **1983**, *105*, 6555–6559.
23. Li, X. M.; Zhu, H. W.; Wei, J. Q.; Wang, K. L.; Xu, E. Y.; Li, Z.; Wu, D. H. Determination of Band Gaps of Self-Assembled Carbon Nanotube Films Using Tauc/Davis-Mott Model. *Appl. Phys. A: Mater. Sci. Process.* **2009**, *97*, 341–344.
24. Gao, R. P.; Pan, Z. W.; Wang, Z. L. Work Function at the Tips of Multiwalled Carbon Nanotubes. *Appl. Phys. Lett.* **2001**, *78*, 1757–1759.
25. Eastman, D. E. Photoelectric Work Functions of Transition, Rare-Earth, and Noble Metals. *Phys. Rev. B* **1970**, *2*, 1–2.
26. Lee, S. H.; Lin, W. C.; Chang, C. J.; Huang, C. C.; Liu, C. P.; Kuo, C. H.; Chang, H. Y.; You, Y. W.; Kao, W. L.; Yen, G. J.; *et al.* Effect of the Chemical Composition on the Work Function of Gold Substrates Modified by Binary Self-Assembled Monolayers. *Phys. Chem. Chem. Phys.* **2011**, *13*, 4335–4339.
27. Van der Pauw, L. J. A Method of Measuring the Resistivity and Hall Coefficient on Lamellae of Arbitrary Shape. *Philips Tech. Rev.* **1958**, *20*, 220–224.
28. ASTM. Test Methods for Measuring Resistivity and Hall Coefficient and Determining Hall Mobility in Single-Crystal Semiconductors. ASTM Designation F76. In *Annual Book of ASTM Standards*; American Society for Testing and Materials: Philadelphia, PA, 2011, Vol. 10.04.
29. Durkop, T.; Getty, S. A.; Cobas, E.; Fuhrer, M. S. Extraordinary Mobility in Semiconducting Carbon Nanotubes. *Nano Lett.* **2004**, *4*, 35–39.
30. DuPont Fluoroproducts. *Teflon PTFE Properties Handbook*; Dupont: Wilmington, DE, 2012.

31. Incropera, F. P.; Dewitt, D. P. *Fundamentals of Heat and Mass Transfer*, 5th ed.; John Wiley & Sons: New York, 2001.
32. Hewitt, C. A.; Kaiser, A. B.; Roth, S.; Craps, M.; Czerw, R.; Carroll, D. L. Multilayered Carbon Nanotube/Polymer Composite Based Thermoelectric Fabrics. *Nano Lett.* **2012**, *12*, 1307–1310.
33. Chee, Y. H.; Niknejad, A. M.; Rabaey, J. M. An Ultra-Low-Power Injection Locked Transmitter for Wireless Sensor Networks. *IEEE J. Solid-State Circuits* **2006**, *41*, 1740–1748.
34. Liu, H.; Crooks, R. M. Paper-Based Electrochemical Sensing Platform with Integral Battery and Electrochromic Read-Out. *Anal. Chem.* **2012**, *84*, 2528–2532.